

University of Groningen

Towards MRI-guided flexible needle steering using fiber Bragg grating-based tip tracking

Moreira, Pedro; Boskma, Klaas Jelmer; Misra, Sarthak

Published in:

ICRA 2017 - IEEE International Conference on Robotics and Automation

DOI:

[10.1109/ICRA.2017.7989564](https://doi.org/10.1109/ICRA.2017.7989564)

IMPORTANT NOTE: You are advised to consult the publisher's version (publisher's PDF) if you wish to cite from it. Please check the document version below.

Document Version

Publisher's PDF, also known as Version of record

Publication date:

2017

[Link to publication in University of Groningen/UMCG research database](#)

Citation for published version (APA):

Moreira, P., Boskma, K. J., & Misra, S. (2017). Towards MRI-guided flexible needle steering using fiber Bragg grating-based tip tracking. In *ICRA 2017 - IEEE International Conference on Robotics and Automation* (pp. 4849-4854). [7989564] (Proceedings - IEEE International Conference on Robotics and Automation). Institute of Electrical and Electronics Engineers Inc..
<https://doi.org/10.1109/ICRA.2017.7989564>

Copyright

Other than for strictly personal use, it is not permitted to download or to forward/distribute the text or part of it without the consent of the author(s) and/or copyright holder(s), unless the work is under an open content license (like Creative Commons).

The publication may also be distributed here under the terms of Article 25fa of the Dutch Copyright Act, indicated by the "Taverne" license. More information can be found on the University of Groningen website: <https://www.rug.nl/library/open-access/self-archiving-pure/taverne-amendment>.

Take-down policy

If you believe that this document breaches copyright please contact us providing details, and we will remove access to the work immediately and investigate your claim.

Downloaded from the University of Groningen/UMCG research database (Pure): <http://www.rug.nl/research/portal>. For technical reasons the number of authors shown on this cover page is limited to 10 maximum.

Towards MRI-guided Flexible Needle Steering Using Fiber Bragg Grating-Based Tip Tracking

Pedro Moreira, Klaas Jelmer Boskma and Sarthak Misra

Abstract—The use of magnetic resonance (MR) images for needle-based interventions offers several advantages over other types of imaging modalities (e.g., high tissue contrast and no radiation). However, MR-guided interventions face challenges related to electromagnetic compatibility of medical devices and real-time tracking of surgical instruments. This work presents a flexible needle steering system that combines an MR-compatible robot and a Fiber Bragg Grating (FBG)-based needle tip tracker. The MR images are used to localize obstacles and targets, while the FBG sensors provide strain measurements for online estimation of the needle tip position. A pre-operative planner defines the needle entry point and desired path, while a model predictive controller calculates the needle rotation during the insertion. To the best of the authors knowledge, this is the first work that fuses MR images and FBG-based tracking to steer a flexible needle in closed-loop inside the MR bore. The system is validated by steering a bevel-tipped flexible needle towards a physical target in gelatin phantoms and biological tissues. The needle reaches the target in all trials with an average targeting error of 2.76 mm. Disregarding the target displacement during the insertion, the average targeting error drops to 1.74 mm. The preliminary results demonstrate the feasibility of combining MR images and FBG-based needle tip tracking to steer a flexible needle in clinical procedures. In order to move towards to a clinically-relevant application, the design of a flexible Nitinol biopsy needle is also presented and evaluated by experiments in a prostate of a bull. The flexible needle presented a curvature 2.5 times larger than a conventional biopsy needle while maintaining the ability to collect tissue samples.

I. INTRODUCTION

Needle insertion is a common procedure in minimally invasive surgery. In the last decade, steerable flexible needles were introduced to reduce targeting errors and to allow maneuvers around anatomical obstacles. Bevel-tipped flexible needles naturally bend when they are inserted in soft-tissues and can be steered by rotating their base during the insertion. Manual steering of such a flexible needle is not intuitive, therefore a robotic system is needed to accurately steer the needle towards a target [1].

An accurate needle tip tracker is essential in robot-assisted needle-based interventions. Medical imaging modalities such

Pedro Moreira and Sarthak Misra are affiliated with the Surgical Robotics Laboratory, Department of Biomechanical Engineering, University of Twente, The Netherlands.

Klaas Jelmer Boskma and Sarthak Misra are affiliated with Surgical Robotics Laboratory, Department of Biomedical Engineering, University of Groningen and University Medical Center Groningen, The Netherlands.

This research was supported by funds from the Dutch Ministry of Economic Affairs and the Provinces of Overijssel and Gelderland, within the Pieken in de Delta (PIDON) Initiative, Project MIRIAM (Minimally Invasive Robotics In An MRI environment).

The authors would like to thank Itai Heijmans for his input on the design of the flexible biopsy needle.

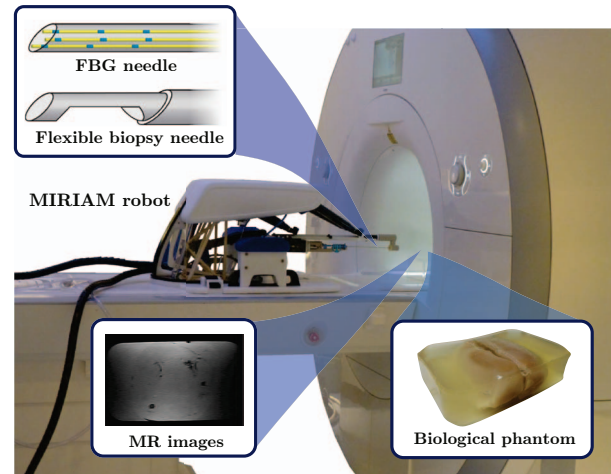


Fig. 1. The MIRIAM robot is an magnetic resonance (MR)-compatible robot that can steer a flexible needle towards a target in biological soft-tissues. The system is capable of inserting, rotating and firing a biopsy needle to collect tissue samples. The needle is integrated with 12 Fiber Bragg Grating (FBG) sensors. The FBG-based needle tip tracking is used to provide the tip position during the insertion, while the MR images are used to define obstacles and target locations.

as ultrasound (US), magnetic resonance (MR), and computed tomography (CT) are often used to provide feedback of the needle tip and target locations during the insertion. US imaging is a popular modality due to its relatively low cost and real-time imaging [2]. However, US images do not present a high tissue contrast and cancerous lesions in early stage might not be visible [3]. CT offers a higher tissue contrast than US, but there are potential risks for the patient and the surgeon related to the exposure to ionizing radiation [4]. MR imaging offers a high tissue contrast without radiation. Real-time MR imaging is needed to track the needle during the insertion, however it has some limitations. Artifacts induced by the needle in the real-time MR images impose additional challenges to implement a needle tip tracker for robotic applications. Moreover, a real-time imaging protocol is not always available and for most scanners it is difficult to interactively control the scan parameters [5]. Therefore, just a few studies have been published so far with MR-guided flexible needle steering.

Patel *et al.* presented one of the few works with MR-guided flexible needle steering [6]. The experiments were performed in homogeneous gelatin phantoms and the needle tip was tracked in image slices of 10 mm, which is unfeasible for experiments in biological tissue. In our previous work, our group has presented an novel MR-compatible robot for prostate biopsies (the MIRIAM robot) [7]. However, due to

the lack of a real-time imaging protocol, the insertion was divided in several steps and an MR scan was performed at the end of each step, increasing the total insertion time. A solution to overcome the lack of an accurate real-time needle tip tracker for MR-guided interventions is the use of Fiber Bragg Grating (FBG) sensors.

The use of FBG-based shape estimation of flexible instruments has been already investigated [8]–[10]. Park *et al.* presented a needle with 6 FBG sensors with a deflection estimation error below 0.4 mm [11]. The needle deflection obtained with the FBG-based estimation was compared with the same information provided by MR images. Roesthuis *et al.* performed the validation of a flexible needle equipped with 12 FBG sensors [12]. The three-dimensional (3D) needle shape was reconstructed and compared with the deflection estimated from camera images and theoretical deflection models. Seifabadi *et al.* presented the design and the initial validation of an MR-compatible needle with 12 FBG sensors with a tracking error of 0.5 mm [5]. However, the experiments were performed outside the MR scanner. Although MR-compatible needles with FBG sensors have already been introduced, no closed-loop experiments inside the MR scanner have been presented so far.

This work presents a novel robot-assisted flexible needle steering that combines MR images and FBG-based needle tracking. The MR images are used to detect the target location, while the FBG-based needle tracker provides the online needle tip position during the insertion. A 9 degrees-of-freedom (DOF) MR-compatible robot is used to insert and rotate the needle within the MR scanner (Fig. 1). MR-guided needle steering experiments in biological tissues are presented in order to evaluate the proposed method. The main contribution of this work is the integration of FBG sensors to steer a flexible needle in the MRI environment. To best of the authors knowledge this is the first experimental evaluation of closed-loop flexible needle steering inside the MRI bore using FBG sensors and a model predictive controller. Additionally, this work also presents and evaluates a novel flexible Nitinol needle designed to collect tissue samples. Although flexible needle steering has been an active research topic in the last decade, most of the previous work presented so far with flexible needles (e.g. [13]–[16]) use a solid Nitinol wire with a bevel tip as a needle, which might have a limited use in a clinical application. Therefore, a clinically-relevant flexible needle is an important step towards the implementation of clinical procedures using such needles.

The paper is organized as follows. Section II introduces the methods for the flexible needle steering using the MR images and the FBG-based estimation. Section III presents the design of the flexible biopsy needle. The experimental results steering the flexible needle in biological tissues and the evaluation of the flexible biopsy needle are presented in Section IV. Finally, Section V provides the conclusions and directions for future work.

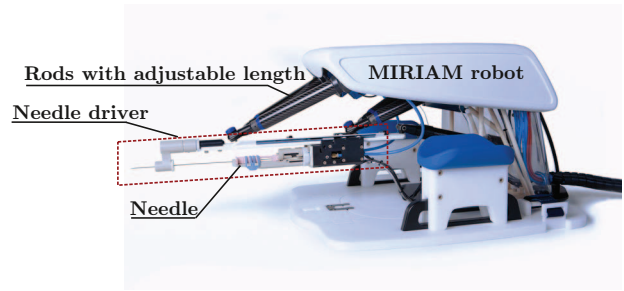


Fig. 2. The MIRIAM robot has five rods with adjustable lengths, which orient the needle driver that is able to insert, rotate and fire the biopsy needle [17].

II. MR- AND FBG-GUIDED NEEDLE STEERING

This section describes the MIRIAM robot, the pre-operative planning, the FBG-based needle tip tracking and the steering controller. The design of a flexible biopsy needle is also presented.

A. MR-Compatible needle insertion robot

The MIRIAM (Minimally Invasive Robotics In An MRI environment) robot is an MR-compatible system primarily designed for prostate biopsies [7]. The robot has 5 rods with adjustable length, which are actuated by piezoelectric motors. The rods provide translational and rotational motion for the needle driver (Fig. 2). The needle driver inserts and rotates the needle using piezoelectric motors and fires the biopsy needle using pneumatic actuation. A control tower containing all the components needed for the robot’s low-level controller (e.g., real-time computer, motor drivers and air compressor) is located in the control room to avoid electromagnetic interference. The robot was already validated in a MAGNETOM Aera 3T scanner (Siemens AG, Germany) and no significant image distortion was observed [7]. The robot operation is supervised from the MR control room through the Graphical User Interface (GUI). The clinician visualizes in the GUI the pre-operative images to select the obstacles and target location, which are used for the pre-operative planning.

B. Pre-operative path planning

The pre-operative path planner defines the best entry point in order to reach the target while avoiding possible obstacles. The clinician selects obstacles and target locations on the pre-operative images displayed in the GUI. The robot is also localised in the pre-operative images (with respect to the fixed MR scanner) using the fiducial located in the needle driver. The algorithm determines the shortest path direction connecting the insertion region and the target. The needle path is then computed along the path direction using a needle deflection model [13]. The model considers the needle deflection as a circular motion in the direction of the bevel tip angle. The planned path (\mathbf{P}) is then represented by a sequence of points along the needle path, such that $\mathbf{P} = [\mathbf{p}_1 \ \mathbf{p}_2 \ \dots \ \mathbf{p}_i]$, where $\mathbf{p}_i \in \mathbb{R}^3$ are the coordinates of each point on the path. If a collision with obstacles occurs, alternative paths are computed by incrementally rotating the original path about the vertical axis. If a viable solution that

Algorithm 1 Pre-operative planner

Input: $(\mathcal{I}_{ins}, \mathbf{p}_{tar}, \mathbf{p}_{obs})$ {Insertion region (\mathcal{I}_{ins}), target (\mathbf{p}_{tar}) and obstacle (\mathbf{p}_{obs}) locations}
 $Dir \leftarrow \text{CheckShortestDirection}(\mathbf{p}_{tar})$
for $\mathbf{p}_{tip} = \mathbf{p}_{tar} : \mathcal{I}_{ins}$ **do**
 $Path \leftarrow \text{NeedleDeflectionModel}(\mathbf{p}_{tip}, Dir)$
end for
if $\text{NoCollision}(Path, \mathbf{p}_{obs})$ **then**
 $EntryPoint \leftarrow \text{CalculateEntryPointAndAngle}(Path)$
 return $EntryPoint$
end if
for $i = 0 : 3000$ **do**
 $PossiblePath(i) \leftarrow \text{ExpandTree}(\mathbf{p}_{tar}, \mathbf{p}_{obs})$
end for
 $Path \leftarrow \text{SelectBestPath}(PossiblePath)$
 $EntryPoint \leftarrow \text{CalculateEntryPointAndAngle}(Path)$
return $EntryPoint$

respects robot constraints and obstacle avoidance cannot be found, an algorithm based on the well-known concept of the rapidly exploring random tree is used. A tree (\mathcal{T}) is expanded from the target location to the insertion region (\mathcal{I}_{ins}) by randomly sampling needle rotations (inputs) and using the same needle deflection model to expand the branches. Any path that arrives at the insertion region without obstacle collision is considered a viable path. The path with the least amount of needle rotations is extracted from the tree and the entry point and robot orientation are calculated. An overview of the pre-operative path planner is presented in Algorithm 1.

C. Needle tip tracking

An accurate needle tip tracking is crucial for a closed-loop flexible needle steering. An FBG-based tracker is used to provide the needle tip pose during the insertion. The experiments are performed with a flexible bevel-tipped Nitinol needle integrated with an array of 12 FBG sensors, divided along three optical fibers. The sensors are co-located in four different locations along the needle shaft (Fig. 3). FBG sensors reflect light of a certain wavelength, which is called the Bragg wavelength. The wave reflection and the grating period is affected by variations in mechanical strains. The shift in the Bragg wavelength is used to calculate the strains at each FBG sensor [12]. An algorithm estimates the curvature and the direction of each group of co-located FBG sensors based on its strains values. The measured strain in each sensor is given by:

$$\epsilon_k(l) = \kappa(l)r_{fn}\sin(\varphi(l) + \alpha_{fn}) + \epsilon_0(l) \quad (1)$$

where l is the distance between the sensor and the needle base, r_{fn} and α_{fn} are the position and orientation of the fiber center at the cross section with fn referring to the fiber number. The curvature ($\kappa(l)$) and its direction ($\varphi(l)$) are computed from the set of measured strains [12]. A spline interpolation is performed to find an approximate value of curvatures and directions along the entire needle.

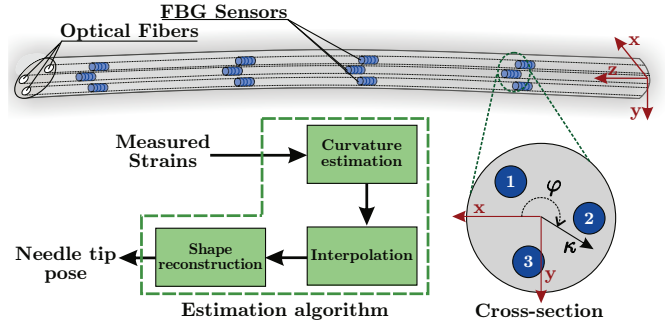


Fig. 3. The Nitinol needle contains three optical fibers, each one with four Fiber Bragg Grating (FBG) sensors. The strains are measured by the reflected light wavelength. The measured strains from the co-located FBG sensors are used as an input for the estimation of the needle curvature (κ) and its direction (φ). The curvature information is used to interpolate and reconstruct the needle shape.

A numerical method is applied to reconstruct the needle shape using a finite number of segments (i) along the entire needle shaft. A series of homogeneous transformation linking the segments along the needle shaft is performed to calculate the needle tip position (\mathbf{p}), so that

$$\begin{bmatrix} \mathbf{p}_{i+1}^0 \\ 1 \end{bmatrix} = \begin{bmatrix} \mathbf{R}_i^0 & \mathbf{p}_i^0 \\ 0 & 1 \end{bmatrix} \begin{bmatrix} \mathbf{p}_{i+1}^i \\ 1 \end{bmatrix}, \quad (2)$$

where $\mathbf{R}_i^0 \in SO(3)$, $\mathbf{p}_i^0 \in \mathbb{R}^3$ and $\mathbf{p}_{i+1}^i \in \mathbb{R}^3$ are the rotation matrix, the element position in the global reference frame and the element position with respect to the previous element, respectively. At each element, the estimated curvature is used to calculate the origin of the next element frame (\mathbf{p}_{i+1}). For further details regarding shape reconstruction, we refer the reader to our previous study [12]. The needle tip position with respect to the fixed MR scanner is calculated by an homogeneous transformation defined by the position and orientation of the needle driver. A Kalman filter is then applied to remove the noise in the position and orientation information, which is used by the needle insertion control as feedback.

D. Needle steering controller

Flexible needles with an asymmetric tip bend when inserted into tissues. Such needles can be steered towards a target by rotating its base [2]. A predictive controller to steer the needle towards a target can be implemented using a needle deflection model and a preplanned path. Consider the discrete needle deflection model as follows [13]:

$$\mathbf{x}_{k+1} = \mathbf{f}(\mathbf{x}_k, u_k), \quad (3)$$

where $\mathbf{x} \in \mathcal{X} \subseteq \mathbb{R}^6$ and $u_k \in \mathcal{U} \subseteq \mathbb{R}$ are the system states (position and orientation of the needle tip) and the system input (needle axial rotation), respectively. The subscript k indicates the discrete index. The constrains \mathcal{X} and \mathcal{U} are given by

$$\mathcal{X} := \{ \mathbf{x} \in \mathbb{R}^6 | \mathbf{x}_{min} \leq \mathbf{x} \leq \mathbf{x}_{max} \}, \quad (4)$$

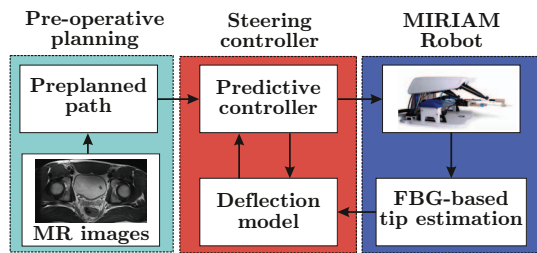


Fig. 4. The overall control architecture used to steer the needle. The pre-operative planner uses the magnetic resonance (MR) images to define the needle entry point and the best needle path. The preplanned path is used by the steering controller, which defines the needle axial rotation. The needle tip position during the insertion is provided by an Fiber Bragg Grating (FBG)-based needle tip tracker.

$$\mathcal{U} := \{u \in \mathbb{R} | u_{min} \leq u_{max}\}. \quad (5)$$

The steering controller defines the needle axial rotation (u_k) to guarantee that the needle will follow the planned path and reach the target. In this work, a 3D steering algorithm based on Nonlinear Model Predictive Controller is implemented to define the needle axial rotation. Such a controller computes the sequence of control inputs ($\mathbf{u} \in \mathbb{R}^{N_p}$) in a prediction horizon ($N_p \in \mathbb{N}^*$) that minimizes a cost function (J_k) that defines the desired system behavior. For the needle steering, the cost function is defined to guarantee that the needle follows the path, while reducing the amount of needle axial rotations. The cost function J_k is then defined as follows:

$$J_k = \sum_{j=1}^{N_p} (\mathbf{x}_{k+j} - \mathbf{p}_{k+j}) \mathbf{W}_e (\mathbf{x}_{k+j} - \mathbf{p}_{k+j}) + \sum_{j=1}^{N_p} w_r u_{k+j}^2, \quad (6)$$

where $\mathbf{W}_e \in \mathbb{R}^3$ is a weight matrix and $w_r \in \mathbb{R}$ is a weight constant. By selecting the values of \mathbf{W}_e and w_r , the controller will prioritize the reduction of the path error or needle rotations. A gradient-based algorithm is used to find the solution for the optimization problem. From the sequence of rotations ($\mathbf{u}_{k+1|k+N_p}$), only the first one is applied. At the end of each iteration the needle is inserted using a fixed insertion step (x_{ins}) and then a new sequence of rotations is computed. Fig. 4 presents an overview of the controller developed to steer a flexible biopsy needle.

III. DESIGN OF A FLEXIBLE BIOPSY NEEDLE

Most of the clinically-approved needles are made of stainless steel because of its high strength and biocompatible properties. Needles (e.g., the BIO-CUT needle from Strylab, Italy) fabricated with non-magnetic materials are also available for MR-guided procedures. The BIO-CUT needle is a standard guillotine-type biopsy needle used for taking samples of tissues in the prostate, kidney and liver. It has a bevel tip, which causes needle deflection during the insertion. However, the clinically-approved needles have lower flexibility and reduced steerability than the Nitinol needles.

The design of a flexible biopsy needle allows for a combination of the steering capabilities of a flexible needle with the ability to take tissue samples as a conventional biopsy

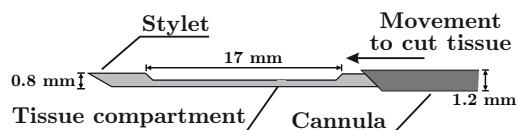


Fig. 5. The biopsy needle consists of a stylet which can be extended and retracted from the cannula. During insertion the stylet is retracted and will be extended at the target site. Following this, the needle cannula is shifted over the stylet so that a tissue sample is obtained, which can be retrieved after the needle retracts.

needle. In this work, an MR-compatible bevel-tipped biopsy needle is designed and evaluated. The outer part (cannula) of the needle is a Nitinol tube with an outer diameter of 1.2 mm and an inner diameter of 1.0 mm. The inner part (stylet) is a Nitinol wire with a diameter of 0.8 mm. Nitinol is chosen due to its biocompatibility and flexibility. The distal end of both cannula and stylet have a bevel tip of 30° (Fig. 5). Different from the BIO-CUT needle, the bevel tip of the cannula and the stylet are parallel in order to increase the needle curvature.

After the needle reaches the target, the stylet pulled out, and then the cannula is fired to collect tissue samples. The indent near the tip of the stylet serves as a tissue compartment. The sharp edges of the compartment helps the cannula to cut the tissue sample. In order to evaluate the performance of the designed flexible biopsy needle, its flexibility and tissue sample size are compared to the BIO-CUT 18G biopsy needle. The results are presented in the following section (Section IV-C).

IV. RESULTS

In this section, we present the experimental plan and results used to evaluate a flexible needle steering controller that combines MR images and FBG-based needle tip tracking. Experiments with the flexible biopsy needle are also presented to demonstrate the feasibility of clinical procedures using flexible Nitinol needles.

A. Experimental plan

The experimental validation of the system is divided into two groups. The first group of experiments validates the needle steering controller, while the second group demonstrates the feasibility of using a flexible biopsy needle.

1) *Flexible needle steering*: The flexible needle integrated with 12 FBG sensors is steered towards a physical target, whose location is defined in pre-operative MR images. The experiments are performed in two different phantoms (Fig. 6):

- Case 1: The needle is steered towards a target while avoiding obstacles in a gelatin phantom. The phantom is prepared with a mass ratio of 90% water and 10% gelatin (Dr. Oetker, The Netherlands). The obstacles and targets are spheres of radius 3 mm, fabricated from Polyvinyl chloride (PVC).
- Case 2: The needle is steered towards a target placed inside an *ex-vivo* biological tissue (chicken breast). The biological tissue is embedded in gelatin (same concentration as in Case 1).

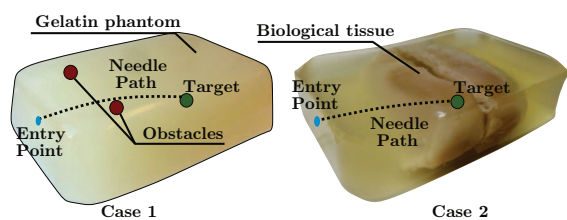


Fig. 6. The experiments are performed in two soft-tissue phantoms. The gelatin phantom from Case 1 (left image) contains obstacles located between the insertion region and the target. The obstacles and targets are made of Polyvinyl chloride (PVC). The biological phantom from Case 2 (right image) is made of gelatin and biological tissue. Spherical targets are embedded inside the chicken breast.

2) *Evaluation of a flexible biopsy needle:* The flexibility of the biopsy needle and BIO-CUT needle are compared by inserting them into a gelatin phantom using the MIRIAM robot. Each needle is inserted 100 mm into the phantom with a constant bevel tip orientation. The gelatin phantom is prepared with a mass ratio of 85% water and 15% gelatin. The capability to collect tissue samples is evaluated by experiments in an *ex-vivo* prostate of a bull. First, the needle is inserted into the prostate, and then the needle is fired using the pneumatic actuation of the robot.

B. Flexible needle steering

Eight insertions trials are performed for each experimental case. The experiments are performed in the Esaote G-Scan Brio scanner (Esaote SpA, Italy) located at the University of Twente and used for research purposes (Fig. 7). MRI scans are acquired with a 3D turbo T1 imaging protocol (TR = 16 ms and TE = 50 ms) with a voxel dimension of 0.70 mm. The scans are performed before and after the experiments for pre-operative planning and final evaluation, respectively. The FBG-based tracking provides the feedback during the insertion and no real-time MR images are used. The path planner defines the best entry point based on the position of obstacles and targets. The needle insertion starts after the robot positions the needle driver at the desired entry point. The steering controller is tuned with an insertion step (x_{ins}) of 3 mm and a prediction horizon (N_p) of 7 iterations. The weighting matrix (\mathbf{W}_e) has its diagonal values set to 10, while w_r is set to 2. These gain parameters are chosen for optimal steering results.

Fig. 7 shows a representative result of insertions in gelatin phantom and biological tissue. The needle appears in the images thicker than its own diameter due to the induced artifact around the needle shaft. The needle reaches the target in all 16 trials, with a average targeting error and standard deviation of 1.95 ± 0.38 mm for Case 1 (gelatin phantom with the obstacles) and 1.53 ± 0.67 mm for Case 2 (biological tissue). The targeting error is calculated based on the information provided by the FBG-based tip tracker, where the error is the distance between the needle tip position and the target location defined in the pre-operative MR images. The targeting error is also calculated based on the MR images acquired after the insertion in order to evaluate the influence of target motion. A set of axial MR images visualizes the

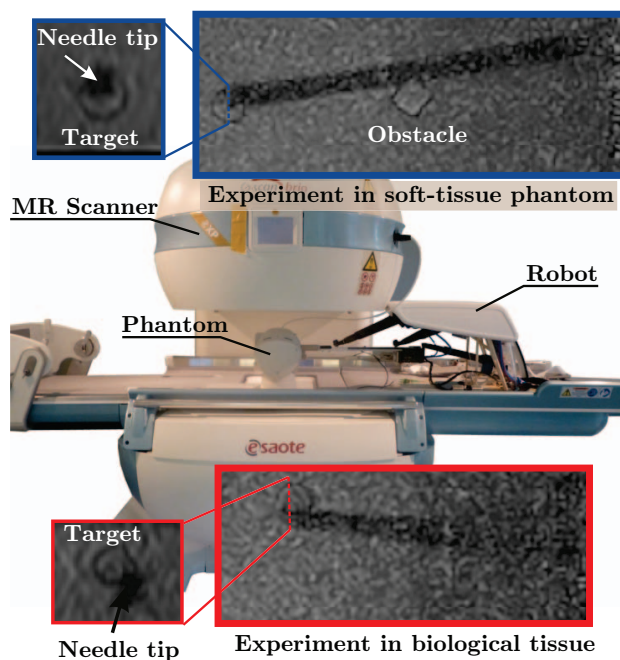


Fig. 7. The experiments are performed in the magnetic resonance (MR) Esaote G-Scan Brio scanner (Esaote SpA, Italy). One representative insertion of each experimental case is presented. The blue inset (top image) shows one insertion into a soft-tissue phantom with obstacles. The needle reached the target location while avoiding a obstacle. The dashed blue inset shows the cross-sectional view of the target after the needle insertion. The red inset (bottom image) shows one representative insertion into biological tissues. The dashed inset shows the cross-sectional view of the target.

cross-section of the target to calculate the Euclidean distance between the needle tip position and the center of the target. The error calculated by the MR images is larger than the FBG-based targeting error due to the displacement of the target during the insertion. The needle tip pushes the target before puncturing it because of the stiffness of the PVC target. The average targeting error and standard deviation calculated by the MR images are 2.33 ± 0.41 mm for Case 1 (gelatin phantom with the obstacles) and 3.19 ± 0.67 mm for Case 2 (biological tissue). These are preliminary results obtained in the Esaote G-Scan Brio due to the availability of the scanner. The MR-compatibility of the MIRIAM robot have already been validated in the 3T MAGNETOM Aera scanner [7]. The larger field of view of the 3T scanner will facilitate the visualization of the robot fiducial and targets in the same set of images. Using such a 3T scanner will reduce the errors associated to the detection of the target location with respect to the robot, hence improving the targeting accuracy.

C. Evaluation of a flexible biopsy needle

Five insertions into a gelatin soft-tissue phantom are performed using the designed flexible biopsy needle. The results are compared with the performance of the clinically-approved BIO-CUT needle. The needles are inserted 100 mm inside the phantom using the MIRIAM robot with a constant orientation. The deflection of the needle from a straight path is then measured. The average deflection and its standard deviation obtained with the flexible biopsy needle

is 20.72 ± 1.03 mm, while using the BIO-CUT needle is 8.32 ± 1.07 mm. The flexible needle has a curvature 2.5 times larger than the BIO-CUT needle, which results in a greater steerability. A t-test demonstrates that the result with the two needles is statistically significant ($p < 0.0001$).

In addition to the curvature analysis, the needle is also tested to evaluate its capability to collect tissue sample. The length of the tissue sample collected from a prostate of bull is measured in 5 trials for each needle (Fig. 8). An average tissue sample length of 6.76 ± 2.11 mm and 6.38 ± 1.58 mm are obtained for the BIO-CUT and the flexible biopsy needles, respectively. The lack of vascularization and internal pressure in *ex-vivo* tissues impairs the amount of material collected in both cases. A t-test shows that the difference in tissue sample size is statistically not significant ($p = 0.7807$).

V. CONCLUSIONS

In this work, we present flexible needle steering that combines MR images and FBG-based needle tip tracking. The system integrates an MR-compatible robot with a pre-operative planner and a needle steering algorithm. The model predictive controller uses the feedback provided by the FBG-based tip tracker to steer the needle in biological tissue. The system is evaluated with experiments in gelatin phantoms and biological tissues. In all 16 trials the needle tip reaches the target and the average targeting errors calculated by the FBG-based tip tracker is 1.74 mm, which is within the range of the smallest clinically significant prostate tumor (diameter of 5 mm) [18]. The feasibility of performing clinical procedures with flexible needles, such as biopsies, is demonstrated using the novel flexible biopsy needle design. The needle flexibility and ability to collect tissue samples are tested and compared to a clinically-approved needle. The flexible needle presented the same capability to collect tissue samples and a curvature 2.5 times larger than the clinically-approved needle.

Future work will focus on implementing a real-time MR imaging protocol to estimate target motion during the procedure and improve targeting accuracy. Such a protocol can also be used to develop a needle tip tracker that fuses real-time MR images and FBG sensors, increasing the reliability of the system. In addition, we are currently integrating the FBG-sensors in the flexible biopsy needle. Cadavers and animal studies are also planned in order to bring our system closer to the clinical use.

REFERENCES

- [1] M. Abayazid, C. Pacchierotti, P. Moreira, R. Alterovitz, D. Praticchizzo, and S. Misra, "Experimental evaluation of co-manipulated ultrasound-guided flexible needle steering," *International Journal of Medical Robotics and Computer Assisted Surgery*, vol. 12, no. 2, pp. 219–230, 2015.
- [2] M. Abayazid, R. J. Roesthuis, R. Reilink, and S. Misra, "Integrating deflection models and image feedback for real-time flexible needle steering," *IEEE Transactions on Robotics*, vol. 29, no. 2, pp. 542–553, 2013.
- [3] J. J. Fütterer, S. Misra, and K. J. Macura, "MR imaging of the prostate: potential role of robots," *Imaging in Medicine*, vol. 2, no. 5, pp. 583–592, 2010.
- [4] G. Fichtinger, T. L. DeWeese, A. Patriciu, A. Tanacs, D. Mazilu, J. H. Anderson, K. Masamune, R. H. Taylor, and D. Stoianovici, "System for robotically assisted prostate biopsy and therapy with intraoperative CT guidance," *Academic Radiology*, vol. 9, no. 1, pp. 60–74, 2002.

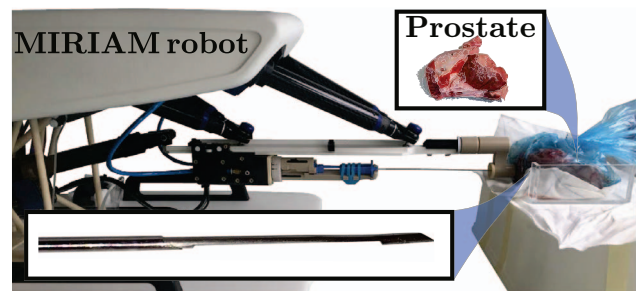


Fig. 8. An *ex-vivo* prostate of a bull is used to evaluate the capability of the needle to collect tissue samples. The needle is inserted into the prostate and fired by the MIRIAM robot.

- [5] R. Seifabadi, E. E. Gomez, F. Aalamifar, G. Fichtinger, and I. Iordachita, "Real-time tracking of a bevel-tip needle with varying insertion depth: Toward teleoperated mri-guided needle steering," in *IEEE/RSJ International Conference on Intelligent Robots and Systems (IROS)*, Nov 2013, pp. 469–476.
- [6] N. A. Patel, T. van Katwijk, G. Li, P. Moreira, W. Shang, S. Misra, and G. S. Fischer, "Closed-loop asymmetric-tip needle steering under continuous intraoperative MRI guidance," in *Proceedings of the IEEE Engineering in Medicine and Biology Society (EMBC)*, 2015, pp. 4869–4874.
- [7] P. Moreira, G. van de Steeg, T. Krabben, J. Zandman, E. E. G. Hekman, F. van der Heijden, R. J. H. Borra, and S. Misra, "Miriam robot: A novel robotic system for mr-guided needle insertion in the prostate," *Journal of Medical Robotics Research (Accepted)*, 2016.
- [8] L. Zhang, J. Qian, Y. Zhang, and L. Shen, "On sdm/wdm fbg sensor net for shape detection of endoscope," in *Proceeding of the IEEE International Conference on Mechatronics and Automation*, 2005, pp. 1986–1991.
- [9] X. Yi, J. Qian, L. Shen, Y. Zhang, and Z. Zhang, "An innovative 3D colonoscope shape sensing sensor based on fbg sensor array," in *Proceedings of the International Conference on Information Acquisition (ICIA)*, 2007, pp. 227–232.
- [10] V. Mishra, N. Singh, U. Tiwari, and P. Kapur, "Fiber grating sensors in medicine: Current and emerging applications," *Sensors and Actuators A: Physical*, vol. 167, no. 2, pp. 279–290, 2011.
- [11] Y. L. Park, S. Elayaperumal, B. Daniel, S. C. Ryu, M. Shin, J. Savall, R. J. Black, B. Moslehi, and M. R. Cutkosky, "Real-time estimation of 3-d needle shape and deflection for mri-guided interventions," *IEEE/ASME Transactions on Mechatronics*, vol. 15, no. 6, pp. 906–915, Dec 2010.
- [12] R. J. Roesthuis, M. Kemp, J. J. van den Dobbela, and S. Misra, "Three-dimensional needle shape reconstruction using an array of fiber bragg grating sensors," *IEEE/ASME Transactions on Mechatronics*, vol. 19, no. 4, pp. 1115–1126, 2014.
- [13] P. Moreira and S. Misra, "Biomechanics-based curvature estimation for ultrasound-guided flexible needle steering in biological tissues," *Annals of Biomedical Engineering*, vol. 43, no. 8, pp. 1716–1726, 2015.
- [14] A. Majewicz, S. P. Marra, M. G. van Vledder, M. Lin, M. A. Choti, D. Y. Song, and A. M. Okamura, "Behavior of tip-steerable needles in *ex vivo* and *in vivo* tissue," *IEEE Transactions on Biomedical Engineering*, vol. 59, no. 10, pp. 2705–2715, 2012.
- [15] M. Bernardes, B. Adorno, P. Poignet, and G. Borges, "Robot-assisted automatic insertion of steerable needles with closed-loop imaging feedback and intraoperative trajectory replanning," *Mechatronics*, vol. 23, no. 6, pp. 630–645, 2013.
- [16] K. B. Reed, R. A. V. Kallem, K. Goldberg, A. M. Okamura, and N. J. Cowan, "Integrated planning and image-guided control for planar needle steering," in *Proceedings of the IEEE RAS and EMBS International Conference on Biomedical Robotics and Biomechatronics (BioRob)*, Scottsdale, USA, October 2008, pp. 819–824.
- [17] P. Moreira and S. Misra, "MR-compatible robot for needle-based prostate interventions," in *Proceedings of the Hamlyn Symposium on Medical Robotics*, 2016, pp. 7–8.
- [18] T. A. Stamey, F. S. Freiha, J. E. McNeal, E. A. Redwine, A. S. Whittemore, and h. P. Schmid, "Localized prostate cancer: relationship of tumor volume to clinical significance for treatment of prostate cancer," *Cancer*, vol. 71, no. S3, pp. 933–938, 1993.